

# Axion and dark photon limits from Crab Nebula high energy gamma-rays

Xiaojun Bi<sup>1,2</sup>, Yu Gao<sup>1,\*</sup>, Jinguang Guo<sup>1,2,†</sup>, Nick Houston<sup>3</sup>, Tianjun Li<sup>4,2</sup>, Fangzhou Xu<sup>5,4</sup>, and Xin Zhang<sup>6,7</sup>

<sup>1</sup> *Key Laboratory of Particle Astrophysics, Institute of High Energy Physics,  
Chinese Academy of Sciences, Beijing, 100049, China*

<sup>2</sup> *School of Physical Sciences, University of Chinese Academy of Sciences, Beijing, 100049, China*

<sup>3</sup> *Institute of Theoretical Physics, College of Applied Science,  
Beijing University of Technology, Beijing 100124, China*

<sup>4</sup> *Key Laboratory of Theoretical Physics, Institute of Theoretical Physics,  
Chinese Academy of Sciences, Beijing 100190, China*

<sup>5</sup> *Institute of Modern Physics, Tsinghua University, Beijing 100084, China*

<sup>6</sup> *Key Laboratory of Computational Astrophysics, National Astronomical Observatories,  
Chinese Academy of Sciences, Beijing, 100012, China and*

<sup>7</sup> *School of Astronomy and Space Science, University of Chinese Academy of Sciences, Beijing 100049, China*

The observation of cosmic sub-PeV gamma-rays from the Crab Nebula opens up the possibility of testing cosmic ray photon transparency at the multi-hundred TeV scale. Assuming no deviation from a source gamma-ray emission due to accelerated electron inverse-Compton scattering, higher event energies can extend constraints on the effects of new physics; We consider oscillation between gamma-rays and axions/dark photons, plus attenuation effects from gamma-ray absorption in the case of dark photon dark matter. Combining the recent AS $\gamma$  and HAWC sub-PeV data with earlier MAGIC and HEGRA data, axion-like particles are most constrained in the  $10^{-7} - 10^{-6}$  eV mass range, where the coupling  $g_{a\gamma}$  is constrained to be below  $1.8 \times 10^{-10} \text{ GeV}^{-1}$ . In comparison, gamma ray flux attenuation due to oscillation with a dark photon leads to a very weak constraint on the mixing parameter;  $\epsilon \lesssim 0.2$  for dark photon mass between  $10^{-7}$  and  $10^{-6}$  eV. Direct scattering from dark photon dark matter limits  $\epsilon \lesssim 0.01$  for masses between 6 and 400 eV.

## I. INTRODUCTION

Very high energy cosmic photons are crucial astrophysical observational targets, as they can help us to both understand acceleration mechanisms at high energies and identify cosmic ray sources via their directional information. However, very high energy gamma rays above 100 TeV are rare occurrences due to both the scarcity of nearby sources, and the attenuation effect of scattering from the cosmic microwave background, reducing their visibility from distant extra-galactic sources. Recently, the highest sub-PeV gamma rays from the Crab Nebula events were detected by the Tibet AS $\gamma$  experiment [1]. The Crab Nebula is a well-known high energy gamma ray source, arising possibly due to acceleration processes in the magnetized wind created by the central pulsar. High energy gamma rays in the TeV range originating therefrom have been measured by a number of experiments, including HEGRA [2], MAGIC [3], HESS [4], etc. The latest data from Tibet AS $\gamma$  [1] and HAWC [5] increase the observed gamma ray spectrum to energies above 100 TeV.

Besides astrophysical interests, the propagation of extremely high energy gamma rays can test photon interactions from theories beyond the Standard Model (BSM). Well-motivated scenarios include photon mixing into low-mass bosonic states like axions [6] and dark photons [7, 8], photon decay via Lorentz invariance violation [9, 10], etc.

The Crab Nebula is a major Galactic source of high energy gamma rays, and the high energy scale of its gamma ray spectrum is utilized for constraining Lorentz invariance violation [11].

BSM processes often lead to an energy-dependent photon flux reduction that benefits from higher energy scales of observed gamma rays. In this paper we study the attenuation of gamma ray survival probability from three new-physics processes induced by an axion-like pseudoscalar or a dark photon. In comparison with previous cosmic ray measurements, we demonstrate that the newly observed high energy gamma ray data enhances the constraints on photon interactions with these new light bosons.

Originally proposed as a natural solution to the strong CP problem [12–14], the QCD-axion has recently enjoyed increasing enthusiasm as a non-thermal dark matter candidate [15, 16] within a well-motivated yet evasive parameter space: fulfilling the correct relic density requires the axion mass to be around  $10^{-5}$  eV and the decay constant  $f \sim 10^{12}$  GeV. In addition, generalized axion-like particles (ALP) are light pseudoscalars that carry a similar  $\frac{a}{f} F\tilde{F}$  coupling to photons. ALPs are commonly predicted in grand unified and superstring theories but they are not restricted to a particular mass range. The axion and ALPs are being searched for by a number of experiments (see [17] for a recent review). For high energy cosmic gamma rays, ALPs can cause oscillation effects in the presence of galactic magnetic fields, as explored in recent studies on potential spectral distortions from astrophysical gamma ray sources [18–44].

Dark photons  $A_D$  [45, 46] are the gauge bosons of hid-

\* gaoyu@ihep.ac.cn

† guojg@ihep.ac.cn

den sector  $U(1)$  gauge symmetries under which the Standard Model (SM) particles are not directly charged. The dark photons may kinetically mix with the SM photon, allowing normal matter to acquire a small coupling to the mixed state. Such a mixing causes  $A - A_D$  oscillation in the wherecase the dark photon has nonzero mass, which also enables cosmic photons to scatter off environmental dark photons [47], if in particular the dark photon makes up the dark matter in our Universe. Both effects attenuate energetic gamma rays over long propagation distances. A number of studies have been worked on this [48–51].

In the following Sections II - IV we briefly discuss ALP and dark photon induced oscillation and scattering effects on gamma rays. In Section V we analyze the compilation of Tibet AS $\gamma$ , HEGRA, MAGIC and HAWC data, and give new physics limits by testing the attenuation processes, and then finally conclude in Section VI.

## II. PHOTON-ALP OSCILLATION

The ALP  $a$  couples to photon fields with the characteristic coupling

$$\mathcal{L}_{a\gamma\gamma} = -\frac{1}{4f} a F \tilde{F} = \frac{a}{f} \vec{E} \cdot \vec{B}, \quad (1)$$

where  $f$  relates to the axion decay constant  $f_a$  by  $f^{-1} = c_\gamma \alpha / (\pi f_a)$ , in which  $\alpha = 1/137$  is the fine structure constant and  $c_\gamma$  is a model dependent coefficient dependent on the underlying theory, e.g.  $c_\gamma = -0.97$  and  $0.36$  in KSVZ [52, 53] and DFSZ [54, 55] models, respectively. For ALPs, here we focus on  $g_{a\gamma\gamma} \equiv f^{-1}$  as the sole effective parameter for phenomenological purposes. In the presence of an external magnetic field  $B$ , Eq. (1) becomes a mixing term [6] between the ALP and a photon that allows for oscillation between the ALP and photon polarisations. Ignoring birefringence and Cotton-Mouton effects, the simplified mixing matrix can be written as

$$\mathcal{M} \approx \begin{pmatrix} -\omega_{\text{pl}}^2/2\omega & -\omega_{\text{pl}}^2/2\omega & g_{a\gamma\gamma} B_T/2 \\ g_{a\gamma\gamma} B_T/2 & -m_a^2/2\omega \end{pmatrix}, \quad (2)$$

where  $\omega$  is the photon frequency and  $\omega_{\text{pl}} = 4\pi\alpha/m_e$  is the plasma frequency in the presence of free electrons. The oscillation is then governed by the equation

$$\left(\omega - i\frac{d}{dx} + \mathcal{M}\right) \begin{pmatrix} A_\perp \\ A_\parallel \\ a \end{pmatrix} = 0. \quad (3)$$

The components  $A_\perp (A_\parallel)$  denote for photon polarisation perpendicular (parallel) to the magnetic field's projection  $B_T$  in the transverse plane of the photon propagation direction. The conversion probability of initially unpolarized photons into ALPs over a propagation distance  $L$

is [25]

$$P_{\gamma \rightarrow a}(E_\gamma) = \left(1 + \frac{E_c^2}{E_\gamma^2}\right)^{-1} \sin^2 \left( \frac{g_{a\gamma\gamma} B_T L}{2} \sqrt{1 + \frac{E_c^2}{E_\gamma^2}} \right), \quad (4)$$

where an ALP mass dependent energy scale emerges,  $E_c = |m_a^2 - \omega_{\text{pl}}^2|/2g_{a\gamma\gamma} B_T$ . For low-energy gamma rays with  $E_\gamma < E_c$ , the oscillation amplitude is  $\sim E_\gamma^2$  suppressed; at higher energy  $E_\gamma \geq E_c$  the oscillation amplitude becomes saturated. The oscillation period also becomes less  $E_\gamma$  dependent as  $E_\gamma > E_c$ .

The galactic magnetic field consists of a random component with small coherence scales and a large scale regular component. The impact of the former is subdominant due to a short-length randomness that mostly leads to self-cancellation of oscillation effects, and here we only consider a regular Galactic  $B$ -field component as modelled in Ref. [56]. The strength of  $B_T$  is  $\sim 1 \mu\text{G}$  along the 2 kpc distance between the Crab Nebula and the Earth. The Galactic free electron density is estimated to  $0.1\text{cm}^{-3}$ , leading to a typical energy scale

$$E_c \sim 100 \text{ TeV} \cdot \left(\frac{m_a}{\mu\text{eV}}\right)^2 \left(\frac{g_{a\gamma\gamma}}{10^{-10}\text{GeV}^{-1}}\right)^{-1}, \quad (5)$$

at which the oscillation  $a \leftrightarrow \gamma$  effect becomes manifest in the energy spectrum. The reference  $g_{a\gamma\gamma} = 10^{-10} \text{ GeV}^{-1}$  is the typical scale of constraints from helioscope [57] and cosmic ray searches. As we will show later in Sec. V, the 100+ TeV data from the Crab Nebula also probe  $g_{a\gamma\gamma}$  to this level for ALPs heavier than previous gamma ray data.

Including the oscillation effect, the observed gamma ray flux is then

$$\frac{d\phi}{dE_\gamma} = (1 - P_{\gamma \rightarrow a}) \cdot f_{\text{att.}} \cdot \left. \frac{d\phi}{dE_\gamma} \right|_{\text{source}}, \quad (6)$$

where  $f_{\text{att.}}$  denotes for astrophysical flux attenuation due to gamma ray scattering with the Galaxy's dust and radiation field. Since the Crab Nebula is relatively close to the Earth, SM-induced effects on the visibility of  $\mathcal{O}(10^2)$  TeV gamma rays are marginal [58], and so we simply take  $f_{\text{att.}} = 1$  in the  $\gamma$ -DM scattering scenario.

## III. PHOTON-DARK PHOTON OSCILLATION

In extensions of the SM featuring dark photons  $\gamma'$  with vector  $U(1)$  potential  $A_D^\mu$ , their interactions are introduced via terms of the type

$$\mathcal{L}_{SM \otimes D} = -\epsilon e J_\mu^{SM} A_D^\mu, \quad (7)$$

where  $\epsilon$  is a dimensionless mixing parameter, and  $J_\mu^{SM}$  the SM's electromagnetic current [59]. At energies above that of the dark photon mass but below that of the corresponding fermion mass, these operators can be integrated

out to yield the familiar low-energy interactions

$$\mathcal{L} \supset -\frac{1}{4}\mathcal{F}^{\mu\nu}\mathcal{F}_{\mu\nu} - \frac{\epsilon}{2}\mathcal{F}^{\mu\nu}\mathcal{F}'_{\mu\nu} - \frac{1}{4}\mathcal{F}'^{\mu\nu}\mathcal{F}'_{\mu\nu}. \quad (8)$$

To the lowest non-trivial order in  $\alpha$  and  $\epsilon$  and in the absence of external electromagnetic fields, the corresponding mixing matrix is

$$\mathcal{M} \approx \begin{pmatrix} \Delta_{\text{pl}} & \epsilon\Delta_{\text{pl}} \\ \epsilon\Delta_{\text{pl}} & \Delta_{\text{D}} \end{pmatrix}, \quad \Delta_{\text{pl}} = -\frac{w_{\text{pl}}^2}{2\omega}, \quad \Delta_{\text{D}} = -\frac{m_{\text{D}}^2}{2\omega}, \quad (9)$$

where  $m_{\text{D}}$  is the dark photon mass. The off-diagonal mixing term is nonzero with the presence of charge density along the propagation path. For each polarisation state photon/dark photon oscillation is then governed by the equation

$$(\omega - i\frac{d}{dx} + \mathcal{M}) \begin{pmatrix} A \\ A_{\text{D}} \end{pmatrix} = 0. \quad (10)$$

Solving these equations of motion we find a conversion probability

$$P_{\gamma \rightarrow \gamma'} = 4\epsilon^2 \left( \frac{\Delta_{\text{D}}}{\Delta_{\text{pl}} - \Delta_{\text{D}}} \right)^2 \sin^2 \left[ \frac{(\Delta_{\text{pl}} - \Delta_{\text{D}})x}{2} \right], \quad (11)$$

which results in the oscillation length

$$L_{\text{osc}} = \frac{4\pi\omega}{m_{\text{D}}^2} \simeq 8 \left( \frac{\omega}{100 \text{ TeV}} \right) \left( \frac{\mu\text{eV}}{m_{\text{D}}} \right)^2 \text{ kpc}. \quad (12)$$

By analogy to the axion case discussed in the previous section, upon the inclusion of oscillation effects the observed gamma ray flux is then

$$\frac{d\phi}{dE_{\gamma}} = (1 - P_{\gamma \rightarrow \gamma'}) \cdot f_{\text{att.}} \cdot \left. \frac{d\phi}{dE_{\gamma}} \right|_{\text{source}}. \quad (13)$$

#### IV. DARK PHOTON SCATTERING

Owing to their mixing with ordinary photons, if the dark photon is massive the scattering process  $\gamma\gamma' \rightarrow e^+e^-$  kinematically opens up for gamma rays above the energy threshold

$$E_{\gamma} > E_{\text{th}} = \frac{2m_e^2}{m_{\text{D}}}, \quad (14)$$

and  $10^2$  TeV gamma rays reach this threshold for  $m_{\text{D}}$  down to  $10^{-3}$  eV scale. At the leading order the cosmic ray photon can scatter from the two transversely polarized dark photon modes due to a coupling to electron via mixing with the QED photon. The corresponding Feynman diagrams are shown in Fig. 1. The resulting scattering cross-section is

$$\sigma = \frac{8\pi\epsilon^2\alpha^2}{3(s - m_{\text{D}}^2)^3} \left[ -\beta(s^2 + 4sm_e^2 + m_{\text{D}}^4) + (s^2 + 4sm_e^2 + m_{\text{D}}^4 - 4m_{\text{D}}^2m_e^2 - 8m_e^4) \ln \left( \frac{1 + \beta}{1 - \beta} \right) \right], \quad (15)$$

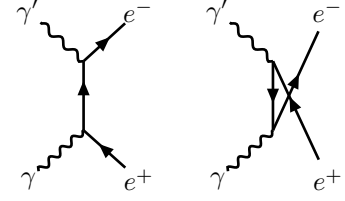


FIG. 1. Photon attenuation diagrams for  $\gamma - \gamma'$  scattering.

where  $\beta = \sqrt{1 - \frac{4m_e^2}{s}}$ ,  $\alpha$  is the fine structure constant,  $m_e$  the electron mass and  $s = 2E_{\gamma}M_{\text{D}}$  is the usual Mandelstam variable. Eq. (16) reduces to photon-photon scattering cross-section up to a factor  $2\epsilon^2/3$  when  $m_{\text{D}} = 0$  due to the absence of the longitudinal mode of the photon.

If the dark photon makes up the major component of the cold dark matter in our Universe the corresponding mean free path of photon propagation is

$$\lambda(E_{\gamma}) = \frac{1}{n_{\text{D}}\sigma}, \quad (16)$$

where the dark photon density  $n_{\text{D}} = \rho_{\text{DM}}/m_{\text{D}}$  follows from that of the Galactic dark matter distribution,  $\rho = 0.3 \text{ GeV cm}^{-3}$ . This being the case we can follow Eq. (13) and calculate the resulting modification of the Crab Nebula gamma ray spectrum via extra scattering attenuation

$$f_{\text{att.}} \rightarrow f_{\text{att.}}^{\text{SM}} \cdot e^{-L/\lambda(E_{\gamma})}, \quad (17)$$

where  $L$  is the distance from Earth to the Crab Nebula.

#### V. FITS TO GAMMA RAYS

To constrain oscillation effects we consider a combination of the recent 100+ TeV gamma ray data from Tibet AS $\gamma$  [1] and HAWC [5], together with previous measurements from HEGRA [2] and MAGIC [3]. The observed gamma ray spectrum is consistent with an expected Inverse-Compton (IC) emission spectrum from accelerated electrons inside the magnetized nebula. The shape of such an IC-dominated spectrum is proposed to follow a ‘parabola’ parametrization [60]

$$\frac{d\phi^{\text{IC}}}{dE} = \phi_0 \left( \frac{E}{E_0} \right)^{\alpha + \beta \log_{10}(E/E_0)}, \quad (18)$$

where the best-fit to AS $\gamma$ , HEGRA, MAGIC and HAWC data gives  $\alpha = -2.57$ ,  $\beta = -0.17$ . This best-fit parameters are obtained by minimizing the  $\chi^2$  function of joint fit

$$\chi^2 = \sum_{\alpha} \sum_i \frac{(\Phi_i^{\text{th}} - f_{\alpha} \cdot \Phi_{\alpha,i})^2}{(f_{\alpha} \cdot \delta\Phi_{\alpha,i})^2} + \sum_{\alpha} \frac{(f_{\alpha} - 1)^2}{(\delta f_{\alpha})^2}, \quad (19)$$

where the subscript  $\alpha$  denotes for different experimental data set, and  $i$  for the  $i$ th spectral bin in each set.

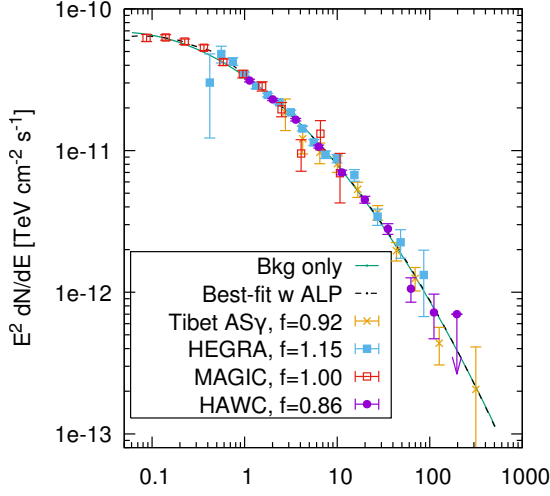


FIG. 2. Background-only fit (solid) and the best-fit with ALP effects (dashed) to Tibet AS $\gamma$  [1], HAWC [5], HEGRA [2] and MAGIC [3] data. The energy scale factor  $f$  is allowed to float for each data set and its best-fit value is listed. Both the IC background (Eq. (18)) and ALP-case achieve good fits with  $\chi^2 = 42.3/42$  and  $\chi^2 = 35.6/38$ , respectively. The ALP best-fit is found to be slightly better than background, although they agree to within  $1\sigma$ .

$\Phi$  is the integrated flux  $E^n d\phi/dE$  in each bin (see Appendix B for detail), where the raised energy-power index  $n$  matches experimental data formats.  $f_\alpha$  is an energy scale uncertainty that accounts for the significant uncertainty in photon energy reconstruction in air shower measurements, which causes the flux spectrum to effectively shift in energy (and magnitude if  $n \neq 1$ ). Such rescaling is typically in the 10-20% range and it is often necessary for the consistency between experiments. The fit with the IC spectrum gives the best scaling factors, as shown in Fig. IV. In our analysis we adopt  $\delta f = 0.15$  for HEGRA [2], 0.15 for MAGIC, 0.12 for Tibet AS $\gamma$  and 0.14 for HAWC. We restrict the variation of  $f_\alpha$  to be within the range of energy scaling uncertainty  $|\Delta f_\alpha| \leq \delta f_\alpha$ .

The fits with axion and dark photon effects are performed after incorporating the photon flux suppression given in Eqs. (6), (13) and (17). For ALP-induced oscillation, a best fit point is obtained at  $g_{a\gamma} = 1.58 \times 10^{-11} \text{ GeV}^{-1}$ ,  $m_a = 1.26 \times 10^{-7} \text{ eV}$  with the minimal  $\chi^2_{\min} = 35.6$ , giving a slight improvement over the background-only fit due to fluctuations in the measured energy spectra.

The fitting process marginalizes over the background IC spectral parameters  $\{\phi_0, E_0, \alpha, \beta\}$  and experimental energy scaling factors  $\{f_\alpha\}$ , to obtain the minimal  $\chi^2$  for each point in the ALP ( $g_{a\gamma}, m_a$ ) and dark photon ( $\kappa, m_{\gamma'}$ ) parameter spaces. The statistical significance of the  $\chi^2$  variation with ALP and  $A'$  parameters needs special treatment due to the highly oscillatory dependence of the spectral deviation on these parameters. Follow-

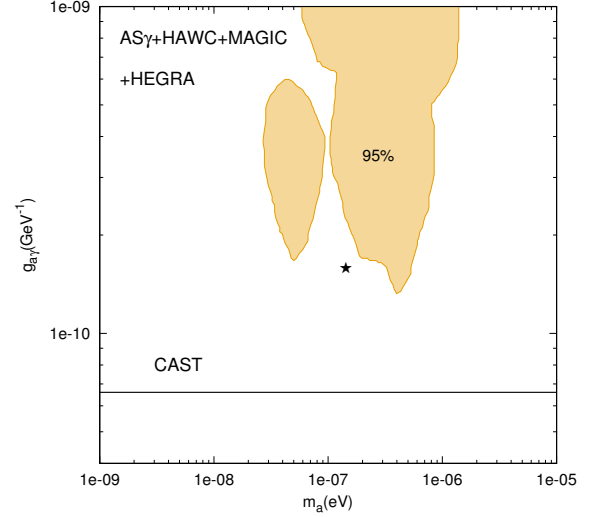


FIG. 3. ALP coupling and mass limits from fitting to Tibet AS $\gamma$ , HAWC, HEGRA and MAGIC data. The filled contours show 95% C.L. exclusion regions with the total  $\chi^2 = 53.4$ . The best fit point  $\chi^2_{\min} = 35.6$  is marked by an asterisk. The CAST limit [57] is shown for comparison.

ing the statistical prescription for nonlinear dependence in Ref. [41], we compare likelihood distribution and find the oscillatory dependence on  $g_{a\gamma}$  and  $m_a$  is equivalent to 3.6 effective degrees of freedom, which corresponds to a 95% C.L. increment  $\Delta\chi^2 \sim 8.8$ .

Interestingly, due to very low global  $\chi^2_{\min}$  value, even with a  $\Delta\chi^2 = 8.8$  increment, a  $\chi^2 = 44.4$  is only slightly worse (at 78% C.L.) than  $1\sigma$  consistency for a  $\chi^2$  distribution with 38 effective degrees of freedom, and this is still a very acceptable global fit. Therefore, we use a more conservative criterion that requires the total  $\chi^2$  to be below 53.4 for 95% consistency with all the data. The resulting exclusion contours on the  $(g_{a\gamma}, m_a)$  plane are shown in Fig. 3. For 95% exclusion around an ALP mass  $10^{-7} - 10^{-6} \text{ eV}$ , the gamma ray data give a limit of  $g_{a\gamma}$  below  $2 \times 10^{-10} \text{ GeV}^{-1}$ , which is close to the latest solar axion constraint from CAST [57].

The 95% C.L. exclusion limit for photon - dark photon oscillation is shown in Fig. 4. Due to a similar oscillatory dependence as in the ALP case, we also estimate 4.6 effective degrees of freedom for the  $\chi^2$  dependence on the dark photon mixing and mass parameters  $\{\epsilon, m_D\}$ . The 95% C.L. exclusion limit is also placed at  $\chi^2 = 52.2$ . Compared to the threshold-enhancement oscillation amplitude in the ALP case, the oscillation amplitude for dark photons is relatively enhanced for  $\Delta_{\text{pl}} \sim \Delta_D$ . However, a very large mixing parameter  $\epsilon$  would be necessary for any spectral alteration to be comparable to experimental uncertainty. The best 95% C.L.  $\epsilon \leq 0.2$  sensitivity is obtained for  $m_D = 10^{-7} - 10^{-6} \text{ eV}$ .

In comparison,  $\gamma$ -ray scattering on dark photon dark matter is relevant at a higher  $m_D$  range near the  $e^+e^-$

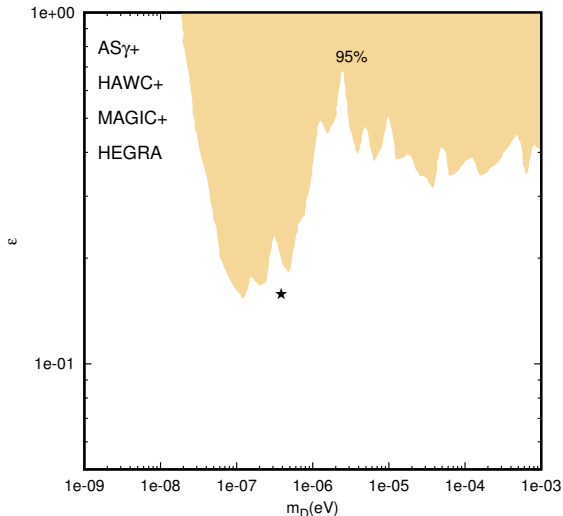


FIG. 4. The 95% C.L. exclusion region for oscillation between gamma-ray and dark photon from fitting to Tibet AS $\gamma$ , HAWC, HEGRA and MAGIC data. The contour denotes  $\chi^2 = 52.2$  with 37 degrees of freedom. The best fit  $\chi^2_{\min} = 35.6$  is marked by the asterisk point.

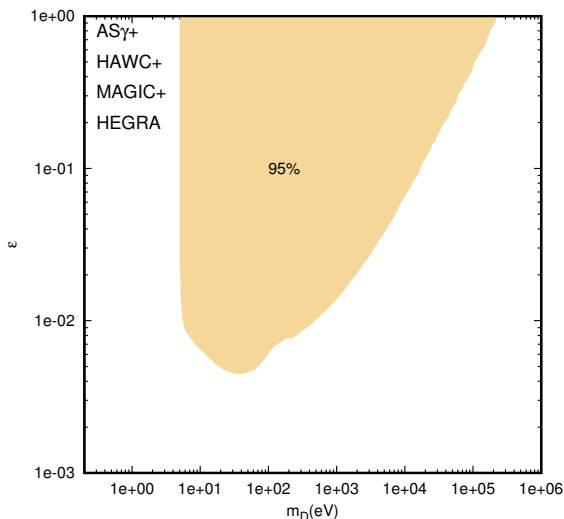


FIG. 5. The 95% C.L. exclusion region for gamma-ray scattering on dark photon as dark matter, from fitting to Tibet AS $\gamma$ , HAWC, HEGRA and MAGIC data.

threshold. Spectral attenuation due to scattering is non-oscillatory, and the 95% C.L. limit in Fig. 5 corresponds to a total  $\chi^2 = 55.8$ . The best exclusion of  $\epsilon > 0.01$  occurs at  $m_D \sim 100$  eV. These dark photon  $\epsilon$  limits are much higher than the typically small mixing required for  $A_D$  to decouple as dark matter, and significantly less stringent than other dark photon constraints [61].

Note the HESS experiment also observes high energy

gamma rays from the Crab Nebula [4], and the resulting spectrum is well fit by the IC background. However, the very low  $\chi^2$  from HESS data is an overfit to the IC background model, and inclusion of this data set in the combined fit would lead to a less stringent constraint on new physics. Therefore, we do not include HESS in Fig. 3. For comparisons, we list the ALP fitting result to individual data set, and the result after including HESS data, in Appendix B.

## VI. CONCLUSION

We have studied potential gamma ray spectral distortions induced by ALPs and dark photons in light of the recent measurement of photons above 100 TeV from the Tibet AS $\gamma$  and HAWC experiments. The newly measured higher energy gamma ray events from the Crab Nebula allow us to extend beyond the sensitivity of previous studies to a higher ALP mass range. Assuming an astrophysical background spectrum from accelerated electron inverse Compton occurring scattering inside the Crab Nebula, we performed analyses on the data consistency with the IC background, including oscillation and attenuation effects from the photon interactions with axion-like particles and dark photons.

The Tibet AS $\gamma$ , HAWC data and previous HESS, MAGIC and HEGRA data are in very good consistency with a single parabola IC background, at the cost of shifting the energy scale of each experiment in a range comparable to their reported energy uncertainties. All of Tibet AS $\gamma$ 's highest energy gamma ray events are from the Crab Nebula. The relatively close distance to the Earth makes the oscillation effects less significant compared to signals from farther away sources, but the higher energies involved can probe into the higher ALP mass range of  $10^{-7} - 10^{-6}$  eV. For a mass region centred at  $2 - 6 \times 10^{-7}$  eV, the ALP-photon effective coupling is excluded to  $1.8 \times 10^{-10}$  GeV $^{-1}$ . These limits may improve with future accumulation of extremely high energy gamma ray data, or 100+ TeV measurements from other identifiable sources at significant distances.

We also studied the effect of high energy gamma ray oscillations into dark photons, and the flux attenuation from scattering on massive dark photons in the form of cold dark matter. Due to kinetic mixing, the propagating modes in  $\gamma - \gamma'$  mixing require a  $U(1)_{\text{EM}}$  breaking medium to develop an effective mass, which leads to relatively suppressed photon - dark photon oscillation effects due to the limited free charge density in the Galactic medium. An  $\epsilon \sim 0.2$  mixing is needed to yield significant modification on the observed gamma ray data for dark photon masses  $m_D > 10^{-7}$  eV. Assuming the dark photon constitutes all the dark matter in our Universe, inclusion of the flux attenuation due to scattering on dark photons also leads to  $\epsilon \sim 0.01$  for  $m_D \sim 100$  eV. Both are subdominant to the existing laboratory and cosmological bounds.

## Acknowledgments

Y.G. thanks the Institute of High Energy Physics, CAS, for support by the grant no. Y95461A0U2 and partially by no. Y7515560U1. T.Li is supported by the National Natural Science Foundation of China under

grant no. 11875062 and 11947302, and by the Key Research Program of Frontier Science, CAS. J.G.Guo is supported by the National Key R&D Program of China (No. 2016YFA0400200), X.J.Bi is supported by NSFC under grant nos.U1738209 and 11851303.

- 
- [1] M. Amenomori et al., Phys. Rev. Lett. **123**, 051101 (2019), arXiv:1906.05521 [astro-ph.HE].
  - [2] F. Aharonian et al. (HEGRA), Astrophys. J. **614**, 897 (2004), arXiv:astro-ph/0407118 [astro-ph].
  - [3] J. Aleksić et al. (MAGIC), Astropart. Phys. **72**, 76 (2016), arXiv:1409.5594 [astro-ph.IM].
  - [4] A. Abramowski et al. (H.E.S.S.), Astron. Astrophys. **562**, L4 (2014), arXiv:1311.3187 [astro-ph.HE].
  - [5] A. U. Abeysekara et al. (HAWC), (2019), arXiv:1905.12518 [astro-ph.HE].
  - [6] G. Raffelt and L. Stodolsky, Phys. Rev. **D37**, 1237 (1988).
  - [7] K. R. Dienes, C. F. Kolda, and J. March-Russell, Nucl. Phys. **B492**, 104 (1997), arXiv:hep-ph/9610479 [hep-ph].
  - [8] S. A. Abel, J. Jaeckel, V. V. Khoze, and A. Ringwald, Phys. Lett. **B666**, 66 (2008), arXiv:hep-ph/0608248 [hep-ph].
  - [9] S. R. Coleman and S. L. Glashow, Phys. Lett. **B405**, 249 (1997), arXiv:hep-ph/9703240 [hep-ph].
  - [10] G. Amelino-Camelia, J. R. Ellis, N. E. Mavromatos, D. V. Nanopoulos, and S. Sarkar, Nature **393**, 763 (1998), arXiv:astro-ph/9712103 [astro-ph].
  - [11] P. Satunin, (2019), arXiv:1906.08221 [astro-ph.HE].
  - [12] J. Preskill, M. B. Wise, and F. Wilczek, Phys. Lett. **120B**, 127 (1983).
  - [13] L. F. Abbott and P. Sikivie, Phys. Lett. **120B**, 133 (1983).
  - [14] M. Dine and W. Fischler, Phys. Lett. **120B**, 137 (1983).
  - [15] W. Hu, R. Barkana, and A. Gruzinov, Phys. Rev. Lett. **85**, 1158 (2000), arXiv:astro-ph/0003365 [astro-ph].
  - [16] L. Hui, J. P. Ostriker, S. Tremaine, and E. Witten, Phys. Rev. **D95**, 043541 (2017), arXiv:1610.08297 [astro-ph.CO].
  - [17] I. G. Irastorza and J. Redondo, Prog. Part. Nucl. Phys. **102**, 89 (2018), arXiv:1801.08127 [hep-ph].
  - [18] C. Csaki, N. Kaloper, M. Peloso, and J. Terning, JCAP **0305**, 005 (2003), arXiv:hep-ph/0302030 [hep-ph].
  - [19] A. De Angelis, M. Roncadelli, and O. Mansutti, Phys. Rev. **D76**, 121301 (2007), arXiv:0707.4312 [astro-ph].
  - [20] A. De Angelis, G. Galanti, and M. Roncadelli, Phys. Rev. **D84**, 105030 (2011), [Erratum: Phys. Rev. **D87**, no.10, 109903 (2013)], arXiv:1106.1132 [astro-ph.HE].
  - [21] M. Simet, D. Hooper, and P. D. Serpico, Phys. Rev. **D77**, 063001 (2008), arXiv:0712.2825 [astro-ph].
  - [22] M. Fairbairn, T. Rashba, and S. V. Troitsky, Phys. Rev. **D84**, 125019 (2011), arXiv:0901.4085 [astro-ph.HE].
  - [23] M. Meyer, D. Horns, and M. Raue, Phys. Rev. **D87**, 035027 (2013), arXiv:1302.1208 [astro-ph.HE].
  - [24] A. Dominguez, M. A. Sanchez-Conde, and F. Prada, JCAP **1111**, 020 (2011), arXiv:1106.1860 [astro-ph.CO].
  - [25] A. Mirizzi and D. Montanino, JCAP **0912**, 004 (2009), arXiv:0911.0015 [astro-ph.HE].
  - [26] A. Mirizzi, G. G. Raffelt, and P. D. Serpico, Phys. Rev. **D76**, 023001 (2007), arXiv:0704.3044 [astro-ph].
  - [27] A. De Angelis, O. Mansutti, M. Persic, and M. Roncadelli, Monthly Notices of the Royal Astronomical Society: Letters **394**, L21 (2009).
  - [28] M. A. Sanchez-Conde, D. Paneque, E. Bloom, F. Prada, and A. Dominguez, Phys. Rev. **D79**, 123511 (2009), arXiv:0905.3270 [astro-ph.CO].
  - [29] A. V. Belikov, L. Goodenough, and D. Hooper, Phys. Rev. **D83**, 063005 (2011), arXiv:1007.4862 [astro-ph.HE].
  - [30] A. Abramowski et al. (H.E.S.S.), Phys. Rev. **D88**, 102003 (2013), arXiv:1311.3148 [astro-ph.HE].
  - [31] R. Reesman and T. P. Walker, JCAP **1408**, 021 (2014), arXiv:1402.2533 [astro-ph.HE].
  - [32] A. Payez, C. Evoli, T. Fischer, M. Giannotti, A. Mirizzi, and A. Ringwald, JCAP **1502**, 006 (2015), arXiv:1410.3747 [astro-ph.HE].
  - [33] B. Berenji, J. Gaskins, and M. Meyer, Phys. Rev. **D93**, 045019 (2016), arXiv:1602.00091 [astro-ph.HE].
  - [34] M. Ajello et al. (Fermi-LAT), Phys. Rev. Lett. **116**, 161101 (2016), arXiv:1603.06978 [astro-ph.HE].
  - [35] M. Meyer, M. Giannotti, A. Mirizzi, J. Conrad, and M. A. Sánchez-Conde, Phys. Rev. Lett. **118**, 011103 (2017), arXiv:1609.02350 [astro-ph.HE].
  - [36] J. Majumdar, F. Calore, and D. Horns, arXiv preprint arXiv:1711.08723 (2017).
  - [37] G. Galanti and M. Roncadelli, JHEAp **20**, 1 (2018), arXiv:1805.12055 [astro-ph.HE].
  - [38] S. Troitsky, Phys. Rev. **D93**, 045014 (2016), arXiv:1507.08640 [astro-ph.HE].
  - [39] K. Kohri and H. Kodama, Phys. Rev. **D96**, 051701 (2017), arXiv:1704.05189 [hep-ph].
  - [40] Y.-F. Liang, C. Zhang, Z.-Q. Xia, L. Feng, Q. Yuan, and Y.-Z. Fan, JCAP **1906**, 042 (2019), arXiv:1804.07186 [hep-ph].
  - [41] C. Zhang, Y.-F. Liang, S. Li, N.-H. Liao, L. Feng, Q. Yuan, Y.-Z. Fan, and Z.-Z. Ren, Phys. Rev. **D97**, 063009 (2018), arXiv:1802.08420 [hep-ph].
  - [42] M. Libanov and S. Troitsky, (2019), arXiv:1908.03084 [astro-ph.HE].
  - [43] G. B. Long, W. P. Lin, P. H. T. Tam, and W. S. Zhu, (2019), arXiv:1912.05309 [astro-ph.HE].
  - [44] Z.-Q. Xia, Y.-F. Liang, L. Feng, Q. Yuan, Y.-Z. Fan, and J. Wu, Phys. Rev. **D100**, 123004 (2019), arXiv:1911.08096 [astro-ph.HE].
  - [45] P. Fayet, Phys. Lett. **95B**, 285 (1980).
  - [46] B. Holdom, Phys. Lett. **166B**, 196 (1986).
  - [47] R. Ruffini, G. V. Vereshchagin, and S. S. Xue, Astrophys. Space Sci. **361**, 82 (2016), arXiv:1503.07749 [astro-ph.HE].
  - [48] A. P. Lobanov, H. S. Zechlin, and D. Horns, Phys. Rev. **D87**, 065004 (2013), arXiv:1211.6268 [astro-ph.CO].
  - [49] A. Caputo, H. Liu, S. Mishra-Sharma, and J. T. Ruderman, (2020), arXiv:2002.05165 [astro-ph.CO].

- [50] A. Mirizzi, J. Redondo, and G. Sigl, JCAP **0903**, 026 (2009), arXiv:0901.0014 [hep-ph].
- [51] H.-S. Zechlin, D. Horns, and J. Redondo, in AIP Conference Proceedings, Vol. 1085 (American Institute of Physics, 2008) pp. 727–730.
- [52] J. E. Kim, Phys. Rev. Lett. **43**, 103 (1979).
- [53] M. A. Shifman, A. I. Vainshtein, and V. I. Zakharov, Nucl. Phys. **B166**, 493 (1980).
- [54] A. R. Zhitnitsky, Sov. J. Nucl. Phys. **31**, 260 (1980), [Yad. Fiz.31,497(1980)].
- [55] M. Dine, W. Fischler, and M. Srednicki, Phys. Lett. **104B**, 199 (1981).
- [56] R. Jansson and G. R. Farrar, Astrophys. J. **761**, L11 (2012), arXiv:1210.7820 [astro-ph.GA].
- [57] V. Anastassopoulos et al. (CAST), Nature Phys. **13**, 584 (2017), arXiv:1705.02290 [hep-ex].
- [58] S. Vernetto and P. Lipari, Phys. Rev. **D94**, 063009 (2016), arXiv:1608.01587 [astro-ph.HE].
- [59] J.-F. Fortin and K. Sinha, (2019), arXiv:1904.08968 [hep-ph].
- [60] D. Zaborov, A. M. Taylor, D. A. Sanchez, J. P. Lenain, and C. Romoli (H.E.S.S.), Proceedings, 6th International Symposium on High-Energy Gamma-Ray Astronomy (Gamma 2016): Heidelberg, Germany, July 11-15, 2016, AIP Conf. Proc. **1792**, 050017 (2017), arXiv:1612.05111 [astro-ph.HE].
- [61] R. Essig, J. A. Jaros, W. Wester, P. H. Adrian, S. Andreas, T. Averett, O. Baker, B. Batell, M. Battaglieri, J. Beacham, et al., arXiv preprint arXiv:1311.0029 (2013).

## Appendix A: Flux binning & scaling

The energy uncertainty of terrestrial cosmic ray experiments is generally non-negligible thus the smearing on the observed energy needs to be incorporated. The energy resolution of AS $\gamma$  ranges from 20% to 40% [1] and we adopt 30% for this analysis. Similarly, the energy resolution for HEGRA, MAGIC and HAWC is taken as  $\delta = 10\%$  [2], 16% [3] and 23% [5] of the detected energy. The observed spectrum is then convoluted with a normally distributed energy around the ‘true’ energy from the incoming spectrum.

For a detector measuring a photon in one energy bin ranging from  $E_0$  to  $E_0 + \Delta E$ , the expected flux is

$$\Delta\phi = \int_{E_0}^{E_0+\Delta E} dE \int_0^\infty A(E', E) \frac{d\phi}{dE'} dE' \quad (\text{A1})$$

where  $E$  and  $E'$  are the observed and ‘true’ cosmic energies,  $A$  is a window function that takes account for  $E'$  being observed at  $E$  with a normally distributed probability of with energy uncertainty  $\delta \cdot E$ , and  $\frac{d\phi}{dE'}$  is the incoming differential energy flux. After integrating over the energy bin the expected flux is,

$$\Delta\phi = \int_0^\infty \tilde{A}(E', E_0, \Delta E) \frac{d\phi}{dE'} dE', \quad (\text{A2})$$

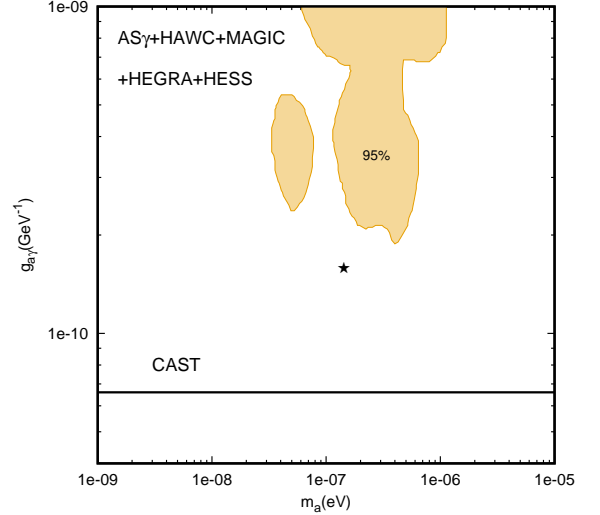


FIG. 6. Similar to Fig. 3, ALP oscillation limits with all five data sets. The total  $\chi^2_{\min} = 57.9$  at the best-fit point (asterisk mark).

where the integrated  $\tilde{A}(E', E_0, E_0 + \Delta E)$  takes the form

$$\tilde{A} = \frac{1}{2} \left[ \text{erf} \left( \frac{E_0 + \Delta E - E'}{\sqrt{2}\delta \cdot E'} \right) - \text{erf} \left( \frac{E_0 - E'}{\sqrt{2}\delta \cdot E'} \right) \right], \quad (\text{A3})$$

where ‘erf’ is the usual Gaussian error function. After spectral smearing, we still need to consider an overall spectral shift due to the experimental energy scaling uncertainty,  $E \rightarrow f \cdot E$ . The flux in an  $f$ -shifted energy bin is

$$\Delta\phi = \int_0^\infty \tilde{A}(E', f \cdot E_0, f \cdot \Delta E) f^n \cdot \frac{d\phi}{dE'} dE'. \quad (\text{A4})$$

Often the experimental data are given in the form of binned flux multiplied by  $E^n$ . Without assumptions on the incoming spectrum, shifted experimental data are treated as  $E^n \frac{d\phi}{dE} \rightarrow f^{n-1} \cdot E^n \frac{d\phi}{dE}$ , maintaining the same event counts in the (shifted) energy bin.

## Appendix B: Comparisons with HESS data

Here we list the IC background fitting result to individual experiments, and also the axion-oscillated fitting results after including HAWC data into the joint analysis.

Table I shows the data’s background consistency with the best fitting results to Inverse Compton spectrum in Eq. 18. The reduced  $\chi^2$  values from AS $\gamma$  and HESS fits are significantly less than one, indicating their combination with other data sets may loosen constraints on spectral distortions. As the new AS $\gamma$  data above 100 TeV are necessary for testing axions at higher mass ranges, we only include AS $\gamma$  in Section V. The five-set joint re-

Data	$\chi^2_{\min}$	d.o.f.	$\phi_0$	$E_0$	$\alpha$	$\beta$
Tibet AS $\gamma$ [1]	1.7	6	$3.19 \times 10^{-13}$	6.28	-2.53	-0.33
HEGRA [2]	13.6	12	$1.58 \times 10^{-12}$	3.02	-2.65	-0.11
MAGIC [3]	6.6	7	$9.96 \times 10^{-13}$	3.79	-2.80	-0.25
HESS [4]	14.8	28	$2.04 \times 10^{-13}$	6.44	-2.79	$-4.06 \times 10^{-3}$
HAWC [5]	6.6	5	$1.01 \times 10^{-11}$	1.77	-2.52	-0.17

TABLE I. Inverse-Compton spectrum fits to each experiment.  $\phi_0$  and  $E_0$  take unit of  $\text{TeV cm}^2\text{s}^{-1}$  and  $\text{TeV}$ .

sult with HESS included is shown in Fig. 6, where the 95% exclusion region moves slightly to larger  $g_{a\gamma}$ .